## PAPER

Check for updates

# Large activation energy in aged Mn-doped Sr$_{0.4}$Ba$_{0.6}$Nb$_2$O$_6$ ferroelectric ceramics

Yingying Zhao, Jiping Wang, [ID]* Lixue Zhang,* Shujuan Liu, Dawei Zhang and Xuan Wang

The properties of ferroelectrics can be significantly enhanced through appropriate doping, and also can be strongly influenced by aging treatment. In this paper, we report a slow aging effect with a large activation energy and an enhanced energy storage density in the aged Mn-doped Sr$_{0.4}$Ba$_{0.6}$Nb$_2$O$_6$ ferroelectric ceramics. Mn-doped Sr$_{0.4}$Ba$_{0.6}$Nb$_2$O$_6$ (SBN40-$x$Mn) ($x$ = 0.0, 1.0, 2.0, 4.0, 6.0, 8.0 mol%) ferroelectric ceramics were prepared by the conventional solid state reaction method. The dielectric constant of Mn-doped Sr$_{0.4}$Ba$_{0.6}$Nb$_2$O$_6$ ceramics shows a decrease after aging in the ferroelectric state. The activation energy derived from the dielectric aging curves shows an obviously large value of 1.87 eV and 2.01 eV for SBN40-4Mn and SBN40-6Mn sample, respectively, compared with the value of 0.55 eV in SBN40-2Mn sample. Besides, the large activation energy is much higher than those values reported in previous literatures for perovskite ferroelectrics such as BaTiO$_3$ and Pb(Ti$_{0.42}$Zr$_{0.58}$)O$_3$ based system. The relaxation time (reflecting the aging rate) is also much longer than the cited perovskite systems. The large relaxation time and activation energy both indicate the slow aging process. Moreover, the aging is related to the migration of oxygen vacancies, and the existence of oxygen vacancies in the Sr$_{0.4}$Ba$_{0.6}$Nb$_2$O$_6$ ceramics is proved by the dielectric relaxation at high temperature and the XPS spectra investigation. Based on the longer relaxation time and larger activation energy, a different diffusion path of oxygen vacancy in our tetragonal tungsten bronze structure high Mn doped SBN is proposed: a long distance migration path of oxygen vacancies among neighbor oxygen octahedron, in contrasting to the short migration distance of oxygen vacancies within perovskite unit cells. In consequence of the long path oxygen vacancy diffusion, a typical double hysteresis loop appeared and the maximum energy storage density is achieved in aged SBN40-4Mn sample. These results can provide guidance for understanding the dynamic of aging process and improving the energy storage properties of doped ferroelectric materials with the tungsten bronze structure.

## Introduction

Ferroelectric materials are widely used in sensors, capacitors, actuators, electro-optical and transducers because of their excellent dielectric, ferroelectric and piezoelectric properties.[1–5] The properties of ferroelectrics can be tailored through the addition of dopants.[6,7] Besides, some dopant like acceptor can induce aging and aging further strongly influences the properties of ferroelectric materials.[8–10] On one hand, during aging the ferroelectric, dielectric and piezoelectric properties of ferroelectric materials will change with time. It is unfavorable to the application of ferroelectric materials.[11,12] On the other hand, there are reports showing that the large recoverable electrostrain can be induced by aging.[13,14] Therefore, it is so important to study the process of aging behavior in the doped ferroelectric materials.

Aging has been reported in many perovskite-type structure ferroelectrics. The deformation of ferroelectric hysteresis loop (including the appearance of constricted or double hysteresis loop) in large signal and the decrease of dielectric properties in small signal are the main characteristic for aged ferroelectrics.[12,14] The double hysteresis loop induced by aging effect has been observed in most acceptor-doped perovskite-type structure ferroelectrics, such as Mn-doped BaTiO$_3$, PbTiO$_3$ and KNbO$_3$-based ceramics.[15–17] The decrease of dielectric properties has been reported in Ba$_{0.6}$Sr$_{0.4}$Nb$_2$O$_6$–Ba$_{0.6}$Sr$_{0.4}$TiO$_3$ (SBN–BST),[18] Ba$_{0.8}$Sr$_{0.2}$TiO$_3$,[19] Ba$_{0.77}$Ca$_{0.23}$TiO$_3$ (ref. 8) systems. Three models have been proposed in explaining the origin of aging process: volume effect, domain wall effect and grain boundary effect. They are all concerned with the migration of oxygen vacancy, which is influenced mostly by the local structure of ferroelectric materials.[11,12,16,20] The investigation of activation energy of oxygen vacancy migration shows that the value is closely related to its moving distance.[19,21,22] In reported acceptor-doped perovskite-type structure ferroelectrics, the activation energy

*State Key Laboratory for Mechanical Behavior of Materials, School of Materials Science and Engineering, Xi'an Jiaotong University, Xi'an 710049, China. E-mail: jpwang@mail.xjtu.edu.cn; lxzhang@mail.xjtu.edu.cn*

value of oxygen vacancy migration is about 1 eV within a short-range distance.[19,21–23]

Strontium barium niobate, $Sr_xBa_{1-x}Nb_2O_6$ (SBN), is a typical lead-free ferroelectric ceramic with a tetragonal tungsten bronze type structure, and has a wide composition range $0.25 \leq x \leq 0.75$. It has received considerable attention due to its high pyroelectric coefficient and piezoelectric constants.[24–26] More importantly, the ferroelectric properties, Curie temperature, as well as the dielectric constant of SBN can be adjusted by changing the Sr/Ba ratio.[27,28] The SBN unit cell formula is $(A1)_2(A2)_4(C)_4(B1)_2(B2)_8O_{30}$. Its Nb atoms occupy the B1 and B2 sites forming $NbO_6$ octahedral parallel to the polar c-axis, which share corners forming three different interstices (A1, A2, and C). A1 is a 12-coordinated tetragonal site and is occupied only by Sr ion. Ba ion and the residual Sr ion occupy the bigger 15-coordinated pentagonal interstice (A2). While there are only five Sr and Ba ions for six A sites, thus one sixth of A sites and the smallest C site are empty.[29–31] For SBN, the study of dopant is mainly about the sintering behavior and the electric properties.[32,33] However, there are only two works investigating the aging behavior and the activation energy of oxygen vacancy diffusion in acceptor-doped tungsten bronze structure ferroelectrics, as far as we know.[18,34] Therefore, further study about the effects of both the dopant and the oxygen vacancy on the aging dynamic in SBN is necessary for understanding the aging of tungsten bronze structure ferroelectrics.

In this paper, we doped Mn in SBN ferroelectric ceramics, which has a tungsten bronze type structure. Moreover, we found a dielectric and polarization aging in the doped SBN samples. Compared with the perovskite ferroelectrics such as 1 mol% Mn-doped $Ba_{0.8}Sr_{0.2}TiO_3$ (ref. 19) and 6 mol% Mn-doped $Pb(Ti_{0.42}Zr_{0.58})O_3$ (ref. 22) (more information shown in subsequent Table 1), a larger activation energy value of the oxygen vacancy migration is revealed in our high Mn doped samples. In consequence, a different migration path of oxygen vacancy is proposed in our study. Our results may provide guidance for the research of aging in tungsten bronze structure ferroelectric ceramics.

## Experimental procedures

### Preparation

$Sr_{0.4}Ba_{0.6}(Nb_{1-x}Mn_x)_2O_6$ ceramics were prepared by the conventional solid state reaction method using $SrCO_3$ (99.9%), $BaCO_3$ (99.9%), $Nb_2O_5$ (99.9%) and $MnO_2$ (99.9%) as starting raw materials ($x$ = 0.0, 1.0, 2.0, 4.0, 6.0, 8.0 mol%). These highly pure chemicals are all from Alfa Aesar company. For convenience, the formula of compositions $Sr_{0.4}Ba_{0.6}(Nb_{1-x}Mn_x)_2O_6$ is abbreviated as SBN40-xMn. The starting materials were weighed according to the stoichiometric formula and ball milled for 4 h. The dried slurries were calcined at 1200 °C for 2 h and then ball milled again for 6 h. After dried at 80 °C, the calcined powders were combined with 10 wt% polyvinyl alcohol (PVA) solution and pressed into disks with a diameter of 12 mm. The disks were sintered at 1300–1370 °C for 4 h. After sintered, the samples were polished and then Ag paint was applied to both faces of the samples, firing at 800 °C for 30 min.

### Characterization

The X-ray diffraction (XRD, X'Pert diffractometer with Cu Kα λ – 0.15406 nm) was used to determine the phase structure of the samples at room temperature. Microstructures of the SBN40-xMn ceramics were observed with a scanning electron microscope (SEM, Hitachi S-2700). The temperature dependence of dielectric constant was measured by HIOKI LCR Hitester at different frequencies over a temperature range of −50–200 °C. The time dependence of dielectric constant was measured by HIOKI LCR Hitester at several aging temperatures (at 1 kHz frequency). The time dependence of polarization-electric field hysteresis loops (P–E hysteresis loops) were characterized by Precision Premier II from Radiant Company, together with a high voltage amplifier. Before each hysteresis loop test and dielectric aging test, a deaging treatment was performed by heating the samples to 200 °C, which is above Curie temperature (43.9–133 °C), and the samples were held for 2 h at 200 °C, then quenched to the aging temperature 25 °C. The P–E hysteresis loops aging time ranges from 1 min to 785 h (about 1 month). Hereafter the aging time of 1 min is denoted as fresh sample state, and the long aging time of 785 h is denoted as the final sample state. The X-ray photoelectron spectroscopy (XPS) spectra were obtained by Axis Ultra (UK) using monochromatic Al Kα (150 W, 15 kV, 1486 eV).

## Results and discussion

### Microstructure

Fig. 1 shows the morphologies of SBN40-xMn ceramics doped with different levels of Mn. It is found that the grains are

**Table 1**  The activation energy of different composites[19,21–23]

| Composites | Structure | Dopant and concentration | Activation energy ($E_a$/eV) | Temperature | Reference | Computing method |
|---|---|---|---|---|---|---|
| $Ba_{0.8}Sr_{0.2}TiO_3$ | Perovskite | 1% Mn | 0.43 | 90–110 °C | 19 | Dielectric permittivity |
| $Pb(Ti,Zr)O_3$ | Perovskite | 0.1% Fe | 0.64 | 40–80 °C | 21 | Phase angle |
| $Pb(Ti_{0.42}Zr_{0.58})O_3$ | Perovskite | 3% Mn | 0.69 | 35–75 °C | 22 | Internal bias |
| $Pb(Ti_{0.42}Zr_{0.58})O_3$ | Perovskite | 6% Mn | 0.64 | 35–75 °C | 22 | Internal bias |
| $Pb(Ti_{0.42}Zr_{0.58})O_3$ | Perovskite | 3% Al | 0.73 | 35–75 °C | 22 | Internal bias |
| $Pb(Ti_{0.42}Zr_{0.58})O_3$ | Perovskite | 6% Al | 0.83 | 35–75 °C | 22 | Internal bias |
| $BaTi_{0.995}Mg_{0.005}O_{2.995}$ | Perovskite | 0.5% Mg | $0.47 \pm 0.04$ | 150–300 °C | 23 | Dielectric losses |
| $Sr_{0.4}Ba_{0.6}Nb_2O_6$ | Tungsten bronze | 2% Mn | 0.55 | 40–55 °C | This work | Dielectric permittivity |
| $Sr_{0.4}Ba_{0.6}Nb_2O_6$ | | 4% Mn | 1.87 | 35–50 °C | This work | |
| $Sr_{0.4}Ba_{0.6}Nb_2O_6$ | | 6% Mn | 2.01 | 35–50 °C | This work | |
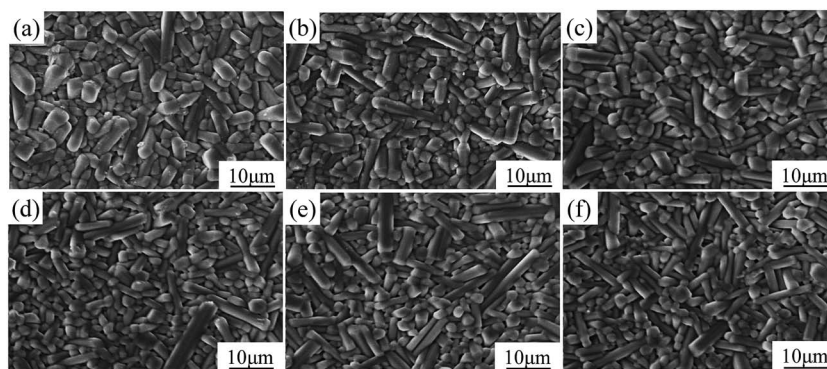
**Fig. 1** The morphologies of SBN40-xMn ceramics: (a) SBN40-0Mn, (b) SBN40-1Mn, (c) SBN40-2Mn, (d) SBN40-4Mn, (e) SBN40-6Mn, (f) SBN40-8Mn.

anisometric and most of them show columnar shape. The grain size does not change much with the Mn content increasing. The columnar shape of the grains may be caused by the growth habit of the tungsten bronze structure. Because the grain growth in (001) facet of tungsten bronze structure is faster due to the lower surface energy.[35]

### XRD patterns results

XRD patterns of SBN40-xMn samples are shown in Fig. 2(a). It can be seen that all the samples show a tetragonal tungsten bronze (TTB) phase without any impurity. Fig. 2(b) shows the variation of the lattice parameters of all the samples with Mn content. With the Mn content increasing, both $a$- and $c$-axis parameters first decrease and then increase. Compared with the lattice parameters of the undoped SBN samples, the lattice parameters of Mn-doped SBN samples change little. That indicates the impossibility of Mn entering into A site to replace Sr/Ba ion, as the big radius difference between Mn ion and Sr/Ba ion can change the lattice parameter obviously.

### Temperature dependence of dielectric constant

Fig. 3 shows the temperature dependence of dielectric constant of SBN40-xMn ceramics measured at different frequencies. With the frequency increasing, the dielectric constant of all the samples decreases. With the temperature increasing, the dielectric constant of all the samples first increases and then

decreases. The temperature of the maximum dielectric constant is the Curie temperature ($T_C$) corresponding to the phase transition from ferroelectric to paraelectric. When the temperature is below $T_C$, the dielectric constants of all the samples show weak frequency dependence. This is caused by the response of different scale domains under different frequencies. When the temperature is above $T_C$, the frequency dependence of dielectric constant increases with the Mn content increasing. Moreover, the dielectric constant of high Mn samples ($x > 2$) shows a strong frequency dependence at temperature above $T_C$. It has been reported that the dielectric relaxation at high temperature is related to the movement of oxygen vacancies.[36,37] This suggests the existence of oxygen vacancy in SBN, which is induced by doping Mn into B site substituting Nb ion. More Mn dopants, more oxygen vacancy generated, so a strong frequency dependence of high Mn samples ($x > 2$) is observed. Besides, the values of $T_C$ are 133.0 °C, 100.4 °C, 96.2 °C, 62.2 °C, 54.0 °C, 43.9 °C for SBN40-0Mn to SBN40-8Mn samples, respectively, which decrease with increasing the Mn concentration.

### Dielectric aging (in a small signal) and the activation energy of oxygen vacancy migration

It is well known that the existence of oxygen vacancy in ferroelectric materials will generate aging effect, such as the decrease of dielectric properties. The time dependence of dielectric constant of SBN40-2Mn, SBN40-4Mn, SBN40-6Mn samples at
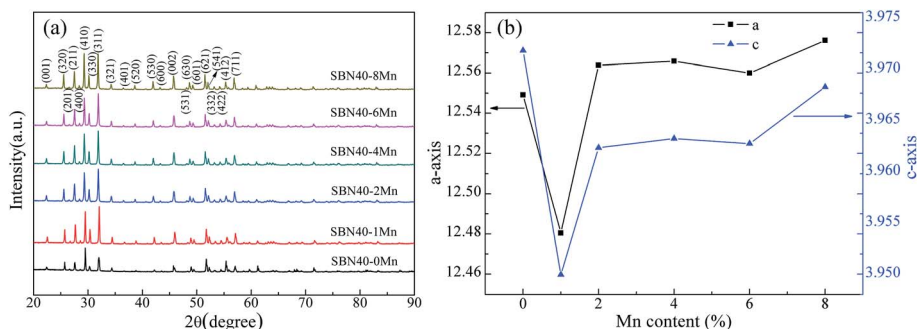


**Fig. 2** (a) XRD patterns, (b) the variation of the lattice parameters of SBN40-xMn ceramics.
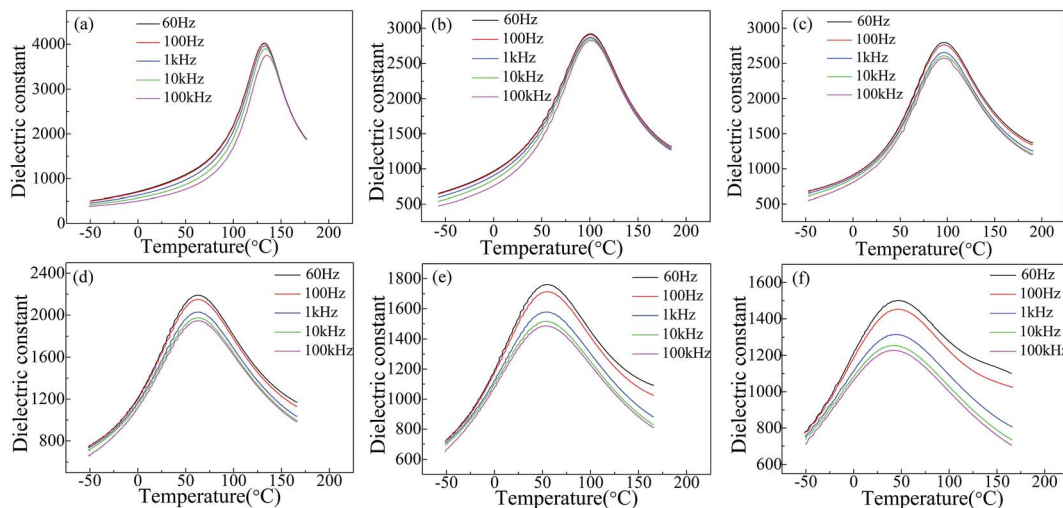
**Fig. 3** Temperature dependence of dielectric constant of SBN40-xMn ceramics: (a) SBN40-0Mn, (b) SBN40-1Mn, (c) SBN40-2Mn, (d) SBN40-4Mn, (e) SBN40-6Mn, (f) SBN40-8Mn.

different temperatures (at 1 kHz frequency) was investigated and the results are shown in Fig. 4(a)–(c). Besides, the time dependence of dielectric constant of SBN40-2Mn, SBN40-4Mn, SBN40-6Mn samples with logarithmic scale for the x axis are shown in Fig. 5(a)–(c). It can be seen that the dielectric constant decreases fast first and then decreases slowly, showing a tendency to be gradually stable after aging 55 h (∼200 000 s).

As the dielectric aging is related to the oxygen vacancy, in order to verify the existence of oxygen vacancy (OV), the O 1s XPS spectra of SBN40-2Mn, SBN40-4Mn, SBN40-6Mn samples were investigated and the results are shown in Fig. 5(d)–(f). The O 1s XPS spectra of all the three samples can be fitted into two peaks. The fitted peak with lower binding energy of about 529.1 eV, denoted by O[1], represents the oxygen in the lattice, while the higher binding energy at about 531.9 eV, denoted by O[2], is assigned to absorbed oxygen species, relating to the presence of oxygen vacancy.[9,38,39] The mole fraction of oxygen vacancy is not given. This is because the oxygen can be affected by many factors such as oxygen in the air, adsorbed oxygen and so on. So the mole fraction of oxygen measured by XPS is inaccurate.

Further, the oxygen vacancy migration influences the dynamics of aging process. It can be seen from Fig. 5(a)–(c) that for different aging temperatures the aging process is different,

which indicated that the aging process is thermally activated. The dielectric aging follows the stretched exponential (or Kohlrausch) function as follows,[40–42]

$$\varepsilon = \varepsilon_\infty + A_1 \exp[-(t/\tau)^\upsilon] \quad (1)$$

where $\tau$ is the relaxation time, which reflects the aging rate. $\upsilon$ denotes the distribution of $\tau$ ($0 \leq \tau \leq 1$), $\varepsilon_\infty$ represents the part which is time independent and the second term on the right-hand side of the equation represents the time dependent part, which becomes zero as $t \to \infty$. As is evident from the solid curves in Fig. 5(a)–(c), which are the fitting curves using eqn (1), the stretched exponential function can describe the experimental data quite well. In the temperature range investigated, the relaxation time can be well described by the Arrhenius behavior.[21] The activation energy ($E_a$) is determined from the relaxation time plot using the Arrhenius relation given as follows,[43–45]

$$\tau_m = \tau_0 \exp(E_a/k_B T) \quad (2)$$

where $\tau_0$ is the pre-exponential factor of the relaxation time, $T$ is the absolute temperature and $k_B$ is the Boltzmann constant. The ln $\tau$ versus $1/T$ plots are shown in Fig. 5(a)–(c) insets and they
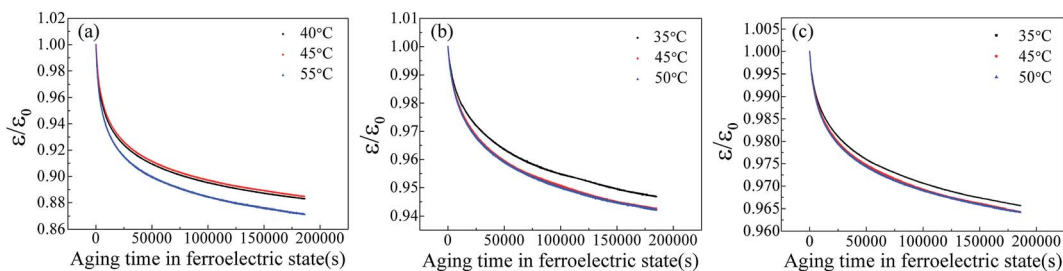


**Fig. 4** The dielectric aging behavior of SBN40-xMn samples at different temperatures (at 1 kHz) (a)–(c): (a) SBN40-2Mn, (b) SBN40-4Mn, (c) SBN40-6Mn.
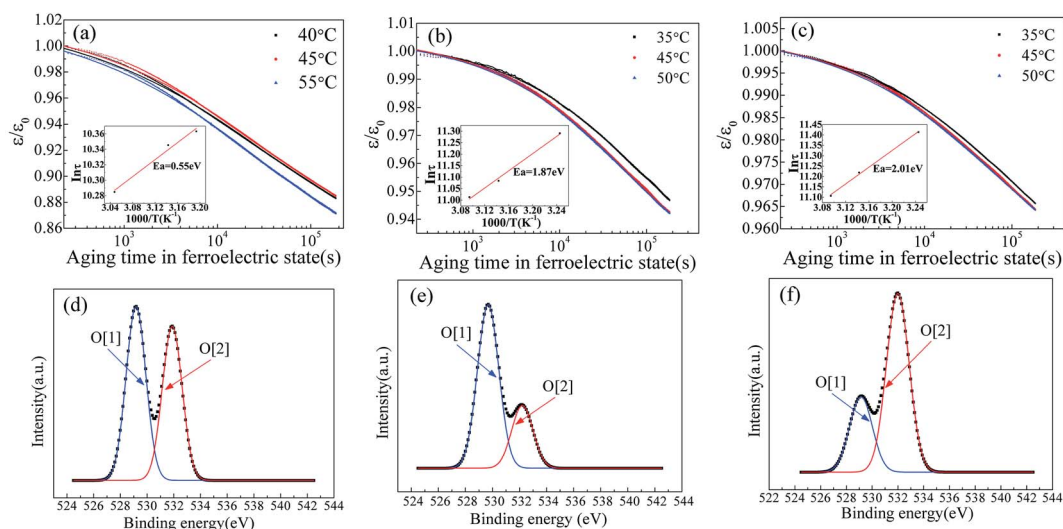
**Fig. 5** Relative changes of dielectric constant of SBN40-$x$Mn samples at different temperatures (at 1 kHz) as a function of time (log scale) (a)−(c): (a) SBN40-2Mn, (b) SBN40-4Mn, (c) SBN40-6Mn (the insets show the Arrhenius plots of ln $\tau$ vs. 1/$T$); the XPS spectra of SBN40-$x$Mn samples (d)−(f): (d) SBN40-2Mn, (e) SBN40-4Mn, (f) SBN40-6Mn.

exhibit a typical Arrhenius behavior. It can be seen that the activation energy value changes with the dopant concentration. Moreover, it is worth mentioning that the activation energy value of 1.87 eV and 2.01 eV differs significantly with the reported values for acceptor-doped perovskite ferroelectrics, such as $BaTiO_3$ doped with Mn and Mg,[19,23] $Pb(Ti,Zr)O_3$ doped with Fe,[21] and $Pb(Ti_{0.42}Zr_{0.58})O_3$ doped with Mn and Al.[22] A summary of the activation energy values of oxygen vacancy diffusion in various reported perovskite systems and our samples are listed in Table 1. It can be found that for perovskite structure ferroelectrics, the activation energy of oxygen vacancy diffusion related to aging is less than 1.0 eV. Meanwhile, in $BaTiO_3$ the activation energy of oxygen vacancy migration is also calculated with a value of 0.91 eV (ref. 46) and 0.99 eV.[47] Comparing the activation energy of SBN in our study with the reported values of perovskite structure ferroelectrics, the activation energy value of 1.87 eV and 2.01 eV in SBN is much larger than the 1.0 eV of perovskite ferroelectrics. Besides, for the $Pb(Ti_{0.42}Zr_{0.58})O_3$ doped with various content of Mn and Al, the activation energy value does not change much with the dopant concentration. This is also contradicted with our results: with Mn content increasing, the activation energy increases from 0.55 eV to 2.01 eV.

For better comparison, the values of relaxation time $\tau$ of SBN40-$x$Mn samples in our work and other reported perovskite systems are shown in Table 2. As shown in Table 2, it is noticed that SBN40-$x$Mn samples show a slow dielectric properties aging with a large relaxation time. On one hand, the relaxation time decreases with temperature increasing. On the other hand, the relaxation time increases with the content of Mn dopant increasing. The increase of relaxation time reflects an increase of activation energy with dopant content.[41] This is in agreement with the results of Fig. 5. Besides, it is worth noting that the relaxation time of our samples is much longer than other reported perovskite ferroelectrics.[40–42]

### The explanation of migration path of oxygen vacancy

It has been reported that for ferroelectrics the change of properties during aging can be explained by the migration of oxygen vacancy.[20,48] Due to the imbalance of valence resulted from the addition of acceptor-dopant Mn ion, the oxygen vacancy would be created.[10] Aging rate is related to the migration time of oxygen vacancy. The acceptor dopant and the oxygen vacancy tend to form a defect dipole rather than remaining isolated during aging.[7] Here we proposed a possible explanation based on a defect dipole volume effect model. Before aging the oxygen vacancy would randomly occupy one of the six sites in $NbO_6$ octahedron. But this state is not stable and the defect dipoles formed by oxygen vacancy associate with Mn ion prefer to align along the spontaneous polarization, and this process is performed with the migration of oxygen vacancy. In the perovskite structure, the oxygen vacancy migration is processed in an oxygen octahedron and its migration path is short. For PZT, oxygen vacancy migrating from a face center to the neighbouring face center require approximately 0.9 eV of activation energy.[49] It can be obtained from reported literatures that the activation energy for oxygen vacancy diffusion in perovskite structure is mostly less than 1 eV or about 1 eV. In ref. 21 and 50, it states that the longer the distance charges move, the larger the activation energy they need. Besides, at high temperature the dielectric relaxation is also involved with the diffusion of oxygen vacancy and the activation energy of oxygen vacancy diffusion is larger with a value between 1–2 eV.[36,37,51] This is due to the dissociation of defect dipole at high temperature and thus the oxygen vacancy could move a long distance.[23]

It is well known that the kinetic migration of oxygen vacancy is closely related to the local structure of ferroelectrics.[16] Based on the above activation energy results, the activation energy for oxygen vacancy migration in our high Mn doped tungsten

**Table 2** The relaxation time of different composites[19,40–42]

| Composites | Structure | Dopant and concentration | Temperature (°C) | Relaxation time (second) | Reference |
|---|---|---|---|---|---|
| $Ba_{0.8}Sr_{0.2}TiO_3$ | Perovskite | 1% Mn | 90 | 4150 | 19 |
| | | | 100 | 3525 | 19 |
| | | | 110 | 2890 | 19 |
| $BaTi_{0.99}Mn_{0.01}O_3$ | Perovskite | 1.5% Ta | 40 | 574.48 | 40 |
| $Na_{0.5}Bi_{0.5}TiO_3$ | Perovskite | 1.5% Fe | 25 | 8817 | 41 |
| $Ba_{0.99}Na_{0.01}TiO_3$ | Perovskite | 1.5% Sm | 40 | 677.71 | 42 |
| $Sr_{0.4}Ba_{0.6}Nb_2O_6$ | Tungsten bronze | 2% Mn | 40 | 31 670 | This work |
| | | | 45 | 31 113 | This work |
| | | | 55 | 29 284 | This work |
| $Sr_{0.4}Ba_{0.6}Nb_2O_6$ | | 4% Mn | 35 | 80 097 | This work |
| | | | 45 | 65 135 | This work |
| | | | 50 | 60 675 | This work |
| $Sr_{0.4}Ba_{0.6}Nb_2O_6$ | | 6% Mn | 35 | 90 577 | This work |
| | | | 45 | 74 527 | This work |
| | | | 50 | 66 638 | This work |

bronze structure SBN is much larger than perovskite ferroelectrics. It indicates that the aging process mechanism of tungsten bronze ferroelectrics may be different from the perovskite structure. For perovskite structure ferroelectrics, the structure is simple. While for SBN, due to its complicated structure with three different interstices, it is reasonable to believe that in tungsten bronze structure the migration path of oxygen vacancy may be different from the perovskite ferroelectrics. In SBN, the oxygen vacancy may move a long distance and it may be conducted with several oxygen octahedron in *ab* plane. The potential migration path of oxygen vacancy in SBN is shown in Fig. 6. For the condition of SBN40-4Mn and SBN40-6Mn samples with activation energy of 1.87 eV and 2.01 eV, respectively, the migration path of oxygen vacancy may cross the triangle and tetragonal interstices as shown in Fig. 6(a) and (b). For the condition of SBN40-2Mn sample with activation energy of 0.55 eV, the migration path of oxygen vacancy is probably similar with perovskite ferroelectrics: (c) within an oxygen octahedron. In addition, because the models interpreting the aging process is still under debate, the oxygen vacancy also may move a long distance to domain walls in the domain boundary model.[18,52] This different migration path of oxygen vacancy might be the explanation for the larger activation energy in SBN.

However, the fundamental reason for the movement path of oxygen vacancy needs further investigation.

### Polarization aging (in a large signal)

It is well known that double ferroelectric hysteresis loop will appear in acceptor-doped ferroelectrics during aging due to the diffusion of oxygen vacancy.[53,54] In order to investigate the polarization aging of SBN, the P–E hysteresis loop evolution after aging different time of all the Mn-doped SBN ceramics are shown in Fig. 7(a)–(f). The samples for measuring P–E hysteresis loop aging were aged at temperature of 25 °C. It can be found that when x < 6% the constrict tendency of P–E hysteresis loop is more and more obvious with increasing the Mn content. This may indicate that the aging effect of doping Mn is strengthened with Mn content increasing. Moreover, when x = 4%, a typical double hysteresis loop induced by migration of oxygen vacancy is observed. Also for all the samples the shape of P–E hysteresis loops is gradually shrinking with the aging time increasing. However, when x > 4%, the P–E hysteresis loops did not show more obvious constricted shape and the shape of P–E hysteresis loop did not change much with the aging time increasing. We consider the reason for the vanishing of double hysteresis loop
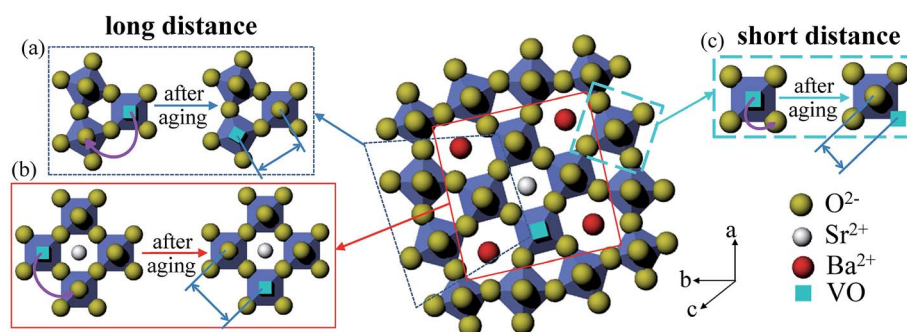


**Fig. 6** The schematic of diffuse paths of oxygen vacancy (VO) during aging in SBN: long-distance migration of oxygen vacancy (a) crossing triangle interstice, (b) crossing tetragonal interstice; short-distance migration of oxygen vacancy (c) migration within an oxygen octahedron.
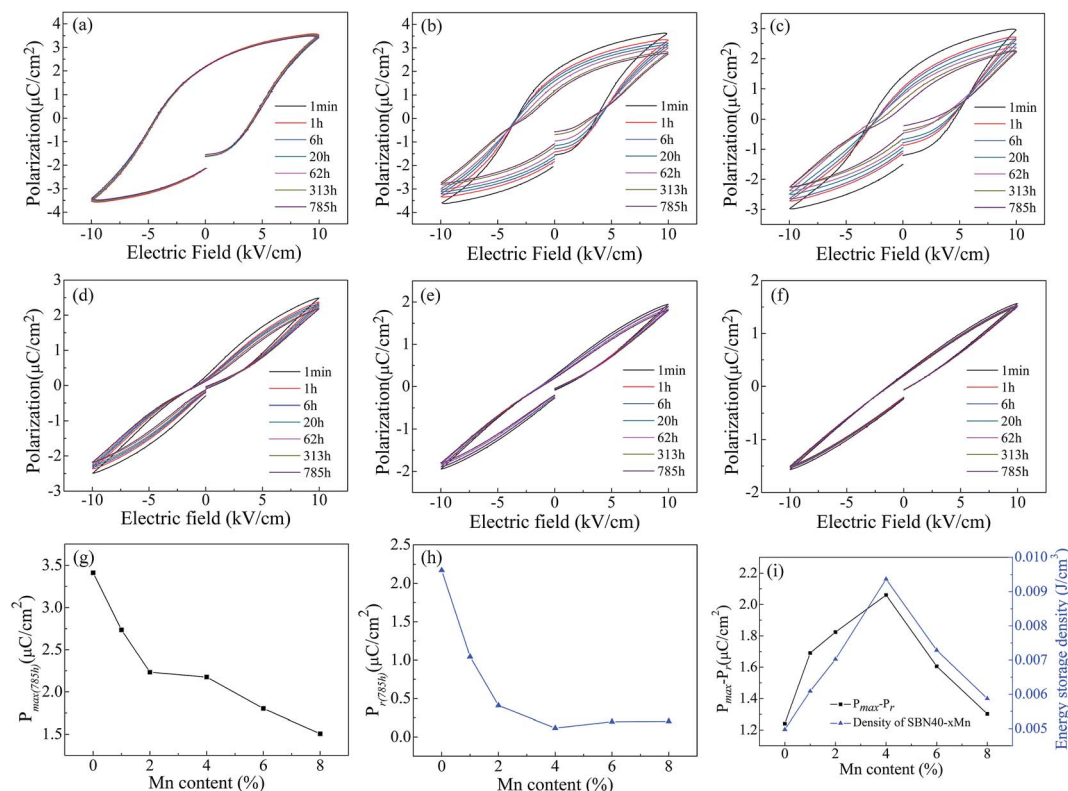
**Fig. 7** $P–E$ hysteresis loop of SBN40−$x$Mn ceramics after aging different time (1 min−785 h) (a)−(f): (a) SBN40-0Mn, (b) SBN40-1Mn, (c) SBN40-2Mn, (d) SBN40-4Mn, (e) SBN40-6Mn, (f) SBN40-8Mn; the changes of $P_{max}$ (g) and $P_r$ (h) after aging 785 h; (i) the $P_{max}−P_r$ and energy storage density after aging 785 h of all the samples.

in higher Mn content sample SBN40-6Mn and SBN40-8Mn is that the aging temperature is close to their Curie temperature. It is well known that the defect polarization $P_D$ will align along the spontaneous polarization $P_S$ and form an internal bias field during aging for the perovskite ferroelectrics. After being applied with an electric field $E$, the $P_S$ will switch to the direction of electric field, while the $P_D$ cannot be switched during such a diffusionless process. After removing the electric field $E$, the $P_D$ will serve as a restoring force making the $P_S$ switch to the original state. As a result, the double $P–E$ hysteresis loop appeared.[11,13,55] When the measuring temperature is nearby the Curie temperature, the decreased degree of lattice deformation leads to a small defect polarization $P_D$, resulting in a small restoring force. After the electric field removed, the $P_S$ cannot switch to the original state with a smaller restoring force, thus the double hysteresis loop is not observed.

The changes of $P_{max}$ and $P_r$ with Mn content after aging 785 h are shown in Fig. 7(g) and (h), respectively. With the Mn content increasing, the $P_{max}$ and $P_r$ decreased. It can be found that SBN40-4Mn sample has the minimum $P_r$ value after aging 785 h. This minimum $P_r$ is considered to be related with the long path oxygen vacancy diffusion. Further analyses on the activation energy of oxygen vacancy diffusion under $P–E$ hysteresis loop measurement are necessary to clarify this consideration. As the polarization is linked to the energy storage density,[56–59] Fig. 7(i) gives the value of $P_{max}−P_r$ and the energy storage density after aging 785 h of all the samples. The

change tendency of $P_{max}−P_r$ value is similar with that of energy storage density. It can be seen that the value of $P_{max}−P_r$ and energy storage density reach the maximum at $x = 4\%$, which has an obvious double hysteresis loop. The reason for the maximum energy storage density can be attributed to the small $P_r$ induced by the aged double hysteresis loops. Therefore, doping Mn and aging treatment are effective measures improving the energy storage density and it is meaningful to the practical application.

## Conclusion

The effects of Mn dopant on the temperature dependence of dielectric properties, dielectric aging (in a small signal) behaviors as well as the fitted activation energy and the polarization aging (in a large signal) of $Sr_{0.4}Ba_{0.6}Nb_2O_6$ ceramics with a tetragonal tungsten bronze structure were investigated. The temperature dependence of the dielectric constant shows a dielectric relaxation at high temperature, which is involved with the existence of oxygen vacancy. And the existence of oxygen vacancy in our $Sr_{0.4}Ba_{0.6}Nb_2O_6$ ceramics is proved by the XPS spectra investigation. The activation energy value of the oxygen vacancy diffusion deduced from dielectric aging ranges from 0.55 eV to an obviously large value of 2.01 eV. Besides, the relaxation time is also much larger (reflecting the aging rate is slow) than that of the compared perovskite systems. Compared with the short migration distance of oxygen vacancy within perovskite unit cell, the possible different migration path of

oxygen vacancy with a longer distance was proposed in higher Mn content SBN samples. A longer migration distance of oxygen vacancy needs a longer time and the corresponding aging rate is slow. The $P$–$E$ loop of the SBN40-4Mn sample shows a double hysteresis loop as aged acceptor-doped perovskite structure ferroelectrics. The polarization aging revealed that when doped with 4 mol% Mn the energy storage density has the peak value. This may provide guidance for the study of dynamic in aging process and improvement of energy storage properties in tungsten bronze structure ferroelectrics.

## Acknowledgements

## References

1 J. Chen, Q. Yun, W. Gao, Y. Bai, C. Nie and S. Zhao, *Mater. Lett.*, 2014, **136**, 11–14.

2 Y. Bai, X. Han, X. C. Zheng and L. Qiao, *Sci. Rep.*, 2013, **3**, 2895.

3 Y. Tan, J. Zhang, Y. Wu, C. Wang, V. Koval, B. Shi, H. Ye, R. McKinnon, G. Viola and H. Yan, *Sci. Rep.*, 2015, **5**, 9953.

4 X. Hao and Y. F. Yang, *J. Mater. Sci.*, 2007, **42**, 3276–3279.

5 W. Li, Z. Xu, R. Chu, P. Fu and G. Zang, *J. Eur. Ceram. Soc.*, 2012, **32**, 517–520.

6 J. Li, R. Huo, R. Guo, F. Li, D. Wang, Y. Tian, Q. Hu, X. Wei, Z. He, Y. Yan and G. Liu, *ACS Appl. Mater. Interfaces*, 2016, **8**, 31109–31119.

7 A. Chandrasekaran, D. Damjanovic, N. Setter and N. Marzari, *Phys. Rev. B: Condens. Matter Mater. Phys.*, 2013, **88**, 214116.

8 Q. Yue, L. Luo, X. Jiang, W. Li and J. Zhou, *J. Alloys Compd.*, 2014, **610**, 276–280.

9 F. Z. Huang, Z. H. Jiang, X. M. Lu, R. X. Ti, H. R. Wu, Y. Kan and J. S. Zhu, *Appl. Phys. Lett.*, 2014, **105**, 022904.

10 E. Sapper, R. Dittmer, D. Damjanovic, E. Erdem, D. J. Keeble, W. Jo, T. Granzow and J. Rödel, *J. Appl. Phys.*, 2014, **116**, 104102.

11 Y. A. Genenko, J. Glaum, M. J. Hoffmann and K. Albe, *Mater. Sci. Eng., B*, 2015, **192**, 52–82.

12 L. Zhang and X. Ren, *Phys. Rev. B: Condens. Matter Mater. Phys.*, 2006, **73**, 094121.

13 Z. Feng and S. W. Or, *J. Alloys Compd.*, 2009, **480**, L29–L32.

14 Z. Li and H. Fan, *Solid State Ionics*, 2009, **180**, 1139–1142.

15 Y. Pu, D. Liu and X. Shi, *Vacuum*, 2014, **99**, 38–41.

16 L. Zhang, W. Liu, W. Chen, X. Ren, J. Sun, E. A. Gurdal, S. O. Ural and K. Uchino, *Appl. Phys. Lett.*, 2012, **101**, 242903.

17 W. Liu, L. Zhang, W. Chen, S. Li and X. Ren, *Appl. Phys. Lett.*, 2011, **99**, 092907.

18 S. Ke, H. Huang, H. Fan, H. L. W. Chan and L. M. Zhou, *J. Phys. D: Appl. Phys.*, 2007, **40**, 6797–6802.

19 D. Xue, J. Gao, L. Zhang, H. Bao, W. Liu, C. Zhou and X. Ren, *Appl. Phys. Lett.*, 2009, **94**, 082902.

20 X. Ren, *Nat. Mater.*, 2004, **3**, 91–94.

21 M. I. Morozov and D. Damjanovic, *J. Appl. Phys.*, 2008, **104**, 034107.

22 K. Carl and K. H. Hardtl, *Ferroelectrics*, 1977, **17**, 473–486.

23 S. H. Cha and Y. H. Han, *J. Appl. Phys.*, 2006, **100**, 104102.

24 Z. Yang, R. Gu, L. Wei and H. Ren, *J. Alloys Compd.*, 2010, **504**, 211–216.

25 I. Bhaumik, S. Ganesamoorthy, R. Bhatt, N. Subramanian, A. K. Karnal, P. K. Gupta, S. Takekawa and K. Kitamura, *J. Alloys Compd.*, 2015, **621**, 26–29.

26 A. S. Bhalla, R. Guo, L. E. Cross, G. Burns, F. H. Dacol and R. R. Neurgaonkar, *Phys. Rev. B: Condens. Matter Mater. Phys.*, 1987, **36**, 2030–2035.

27 M. Said, T. S. Velayutham, W. C. Gan and W. H. Abd Majid, *Ceram. Int.*, 2015, **41**, 7119–7124.

28 J. L. Wang, B. Vilquin, B. Gautier, G. Dezanneau and N. Barrett, *Appl. Phys. Lett.*, 2015, **106**, 242901.

29 C. S. Dandeneau, Y. Yang, B. W. Krueger, M. A. Olmstead, R. K. Bordia and F. S. Ohuchi, *Appl. Phys. Lett.*, 2014, **104**, 101607.

30 A. Belous, O. V'yunov, D. Mishchuk, S. Kamba and D. Nuzhnyy, *J. Appl. Phys.*, 2007, **102**, 014111.

31 T.-T. Fang and H.-Y. Chung, *Appl. Phys. Lett.*, 2009, **94**, 092905.

32 J. T. Shiue and T. T. Fang, *J. Eur. Ceram. Soc.*, 2002, **22**, 1705–1709.

33 T.-T. Fang and F.-Y. Chen, *J. Appl. Phys.*, 2006, **100**, 014110.

34 S. Bu, D. Chun and G. Park, *Jpn. J. Appl. Phys.*, 1997, **36**, 4351–4354.

35 B. Yang, L. Wei, X. Chao, Z. Wang and Z. Yang, *J. Alloys Compd.*, 2015, **632**, 368–375.

36 Z. Yu, C. Ang, P. M. Vilarinho, P. Q. Mantas and J. L. Baptista, *J. Appl. Phys.*, 1998, **83**, 4874.

37 B. S. Kang, S. K. Choi and C. H. Park, *J. Appl. Phys.*, 2003, **94**, 1904.

38 A. B. Hungría, A. Martínez-Arias, M. Fernández-García, A. Iglesias-Juez, A. Guerrero-Ruiz, J. J. Calvino, J. C. Conesa and J. Soria, *Chem. Mater.*, 2003, **15**, 4309–4316.

39 C.-M. Pradier, C. Hinnen, K. Jansson, L. Dahl, M. Nygren and A. Flodstrom, *J. Mater. Sci.*, 1998, **33**, 3187–3191.

40 T. Sareein, M. Unruan, A. Ngamjarurojana, S. Ananta and R. Yimnirun, *Ferroelectrics*, 2014, **458**, 56–63.

41 T. Sareein, M. Unruan, A. Ngamjarurojana, S. Jiansirisomboon, A. Watcharapasorn and R. Yimnirun, *Phys. Lett. A*, 2009, **373**, 1583–1587.

42 T. Sareein, P. Baipaywad, W. Chaiammad, A. Ngamjarurojana, S. Ananta, X. Tan and R. Yimnirun, *Curr. Appl. Phys.*, 2011, **11**, S90–S94.

43 A. Tamilselvan, S. Balakumar, M. Sakar, C. Nayek, P. Murugavel and K. S. Kumar, *Dalton Trans.*, 2014, **43**, 5731–5745.

44 Y. Zhi, A. Chen, P. M. Vilarinho, P. Q. Mantas and J. L. Baptista, *J. Eur. Ceram. Soc.*, 1998, **18**, 1621–1628.

45 Y. Zhi, A. Chen, P. M. Vilarinho, P. Q. Mantas and J. L. Baptista, *J. Eur. Ceram. Soc.*, 1998, **18**, 1629–1635.

46 M. Morozov, Softening and hardening transitions in ferroelectric Pb(Zr,Ti)O$_3$ ceramics, Ph.D. dissertation, École Polytechnique Fédérale de Lausanne, 2005.

47 G. V. Lewis, C. R. A. Catlow and R. E. W. Casselton, *J. Am. Ceram. Soc.*, 1985, **68**, 555–558.

48 L. X. Zhang, W. Chen and X. Ren, *Appl. Phys. Lett.*, 2004, **85**, 5658.

49 S. Gottschalk, H. Hahn, S. Flege and A. G. Balogh, *J. Appl. Phys.*, 2008, **104**, 114106.

50 M. I. Morozov and D. Damjanovic, *J. Appl. Phys.*, 2010, **107**, 034106.

51 O. Bidault, P. Goux, M. Kchikech, M. Belkaoumi and M. Maglione, *Phys. Rev. B: Condens. Matter Mater. Phys.*, 1994, **49**, 7868–7873.

52 Y. Zhou, D. Xue, X. Ding, L. Zhang, J. Sun and X. Ren, *J. Phys.: Condens. Matter*, 2013, **25**, 435901.

53 L. Jin, F. Li and S. Zhang, *J. Am. Ceram. Soc.*, 2014, **97**, 1–27.

54 H. Yan, F. Inam, G. Viola, H. Ning, H. Zhang, Q. Jiang, T. Zeng, Z. Gao and M. J. Reece, *J. Adv. Dielectr.*, 2011, **1**, 107.

55 L. X. Zhang and X. Ren, *Phys. Rev. B: Condens. Matter Mater. Phys.*, 2005, **71**, 174108.

56 B. Qu, H. Du and Z. Yang, *J. Mater. Chem. C*, 2016, **4**, 1795–1803.

57 Q. Zhang, L. Wang, J. Luo, Q. Tang and J. Du, *J. Am. Ceram. Soc.*, 2009, **92**, 1871–1873.

58 L. Wu, X. Wang and L. Li, *J. Am. Ceram. Soc.*, 2016, **99**, 930–937.

59 L. Zhao, Q. Liu, S. Zhang and J.-F. Li, *J. Mater. Chem. C*, 2016, **4**, 8380–8384.